Ferroelectric control of spin and orbital Rashba effects at the Ni/HfO2 interface

Armando Pezo, Andrés Saúl, Aurelien Manchon, Rémi Arras

Letter

Ferroelectric control of spin and orbital Rashba effects at the Ni/HfO_2 interface

Armando Pezo [1,2,*] Andrés Saul [2] Aurélien Manchon,[2] and Rémi Arras [3,†]
[1]*Laboratoire Albert Fert, CNRS, Thales, Université Paris-Saclay, 91767 Palaiseau, France*
[2]*Aix-Marseille Université, CNRS, CINaM, 13009 Marseille, France*
[3]*CEMES, Université de Toulouse, CNRS, 29 rue Jeanne Marvig, F-31055 Toulouse, France*

(Received 21 December 2024; revised 1 March 2025; accepted 28 March 2025; published 9 April 2025)

We predict the giant ferroelectric control of interfacial properties of Ni/HfO_2, namely, (i) the magnetocrystalline anisotropy and (ii) the inverse spin and orbital Rashba effects. The reversible control of magnetic properties using electric gating is a promising route to low-energy consumption magnetic devices, including memories and logic gates. Synthetic multiferroics, composed of a ferroelectric in proximity to a magnet, stand out as a promising platform for such devices. Using a combination of *ab initio* simulations and transport calculations, we demonstrate that reversing the electric polarization modulates the interface magnetocrystalline anisotropy from in-plane to out-of-plane. This modulation compares favorably with recent reports obtained upon electromigration induced by ionic gating. In addition, we find that the current-driven spin and orbital densities at the interface can be modulated by about 50% and 30%, respectively. This giant modulation of the spin-charge and orbit-charge conversion efficiencies opens appealing avenues for voltage-controlled spin- and orbitronics devices.

DOI: 10.1103/PhysRevB.111.L140405

The design of extrinsic multiferroics, formed by the association of a ferroelectric material with a ferromagnet in heterostructures, has been a subject of intense research aiming to obtain large magnetoelectric couplings [1]. Indeed, switching the magnetization by applying an electric field represents an extraordinary opportunity to reduce the power consumption of magnetic memory devices compared to using large magnetic fields or spin-transfer torques. For a few years now, much effort has been devoted to manipulating the magnetization through spin-orbit torques (SOT), which takes advantage of spin currents or densities generated electrically through spin-charge interconversion, i.e., the spin Hall or Rashba-Edelstein effects. These new approaches have led to the emergence of novel logic and memory devices such as the magnetoelectric spin-orbit (MESO) [2], the ferroelectric spin-orbit (FESO) [3] or the SOT-magnetic random access memory (SOT-MRAM) [4] devices.

In these devices, spin-orbit coupling plays a central role as it governs the spin-charge interconversion phenomena. Ferroelectric compounds can substantially boost these mechanisms by altering the crystal structure in a non-volatile manner. Consequently, nonvolatile switching of the spin texture and spin-charge interconversion can be achieved by reversing the ferroelectric polarization using electrical gates [3,5–7]. The structural change accompanying ferroelectric reversal is also expected to alter the orbital transport that has recently dragged attention as a nonrelativistic (spin-orbit coupling-free) alternative to spin transport [8–12]. Therefore, extrinsic multiferroics demonstrating efficient control of the spin and orbital properties are highly desired for low-power consumption devices.

*Contact author: armando-arquimedes.pezo-lopez@cnrs-thales.fr
†Contact author: remi.arras@cemes.fr

However, the use of ferroelectric compounds in miniaturized devices faces several challenges [13]. The electric polarization is indeed known to vanish below a critical thickness when the ferroelectric material is grown in thin films because of the increase of the depolarizing field. A second important problem comes from the fact that the most widely used ferroelectric compounds so far are oxides with a perovskite structure that is difficult to grow on silicon substrates, making them incompatible with complementary-metal-oxide-semiconductor technologies. Of these observations, the recent discovery of ferroelectricity in doped hafnia (HfO_2) films [14–17], which do not suffer from the aforementioned issues, has been welcomed with enthusiasm for the design of ferroelectric-based applications or memories involving resistive-switching processes [18,19].

In spintronic devices, hafnia needs to be incorporated in thin-film heterostructures in which it is interfaced with ferromagnetic metallic electrodes [19]. Several studies have already demonstrated the possibility of controlling the magnetic properties (spin polarization [20], magnetic anisotropy [21], magnetization [22–24]) by reversing the electric polarization in hafnia thin films. In this Letter, using first-principles calculations, we assess the ferroelectric control of spin-orbit properties of Ni/HfO_2 bilayer. We demonstrate that switching the electric polarization not only tunes interfacial magnetism but also modifies the interfacial magnetocrystalline anisotropy from in-plane to out-of-plane. In addition, we show that current-driven spin and orbital densities can be controlled in a nonvolatile manner by ferroelectricity, opening avenues for the gate-controlled spin-charge and orbital-charge interconversion.

To model the effect of the electric polarization on the Ni electrode, we considered a periodic Ni/HfO_2 superlattice, shown in Fig. 1(a) and formed by a total of 20 atomic layers and two interfaces at which the electric polarization P is

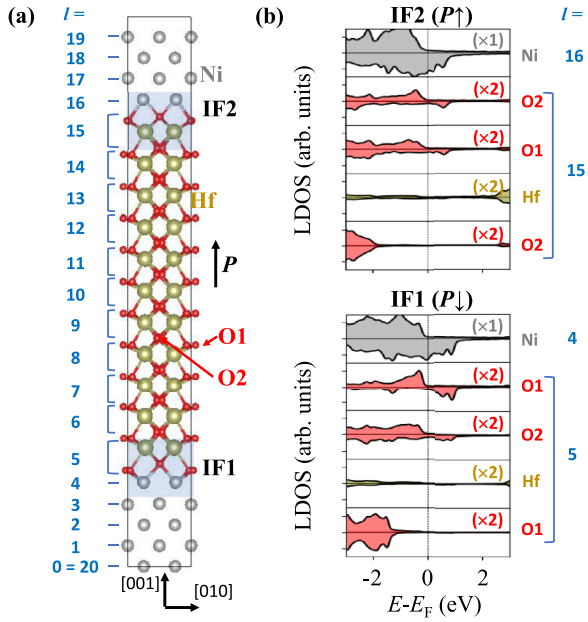

FIG. 1. (a) Atomic structure of the Ni/HfO_2 superlattice used for the calculations, (b) Layer-resolved density of states (LDOS) calculated for the two interfaces IF1 and IF2. Positive and negative DOS correspond to the majority/minority-spin channels, respectively. The LDOSs of HfO_2 atomic layers have been multiplied by 2 for better clarity.

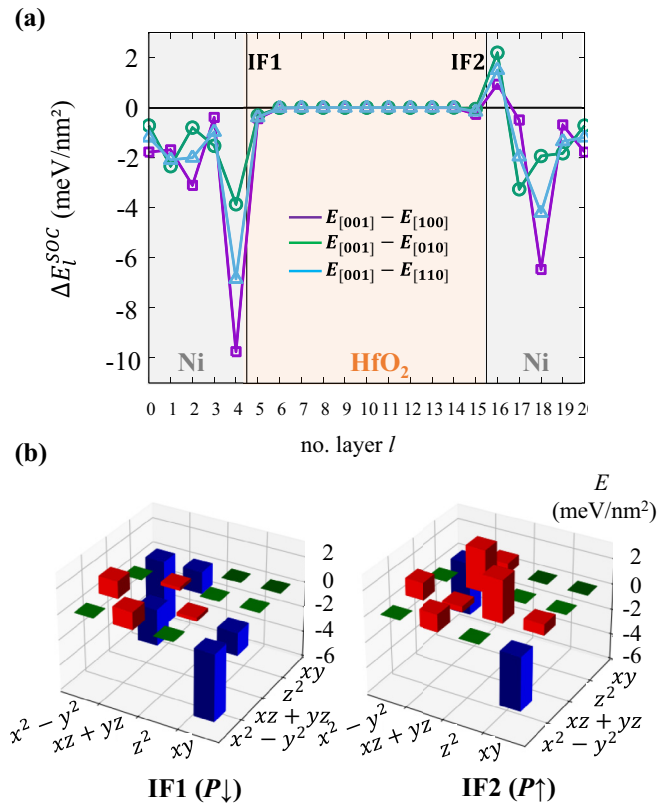

FIG. 2. (a) Layer-resolved MCAE $\Delta E_l^{\mathrm{SOC}}$ calculated for different crystallographic directions, (b) d-orbital contributions to the MCAE of the Ni atoms in the interface layer IF1 ($l = 4$ - P ↓) and IF2 ($l = 16$ - P ↑). The red and blue bars correspond to positive and negative energies.

either pointing inward (P ↓, IF1) or outward (P ↑, IF2). Our numerical investigation is based on the density functional theory and nonequilibrium transport calculations. More details about the numerical methodology and the optimization of the structure are provided in Sec. SI of the Supplemental Material [25].

As can be seen in Fig. 1(a), HfO_2 possesses two inequivalent oxygen atoms, labeled O1 and O2. At the center of the film, the positions of the O1 atoms are off-centered, with a difference of out-of-plane z coordinates between the Hf and O atoms of approximately 27.4 pm. This observation confirms that the electric polarization is stable in the HfO_2 film, although slightly reduced with respect to the bulk value ($\simeq$28.5 pm) due to the presence of a depolarizing field. At the two interfaces, we observe a variation of this difference of z coordinates, which increases up to 27.8 pm at IF1, while it tends to reduce to 25.1 pm at IF2 [see Fig. S1(c) [25]]. As shown in Fig. S1(d) [25], the electric polarization is accompanied by an internal electric field of approximately 1.73×10^8 V m^{-1} that shifts the layer-resolved densities of states (LDOS) higher in energy when moving from layer $l = 6$ to $l = 14$. In Fig. 1(b), we detail the contributions to the LDOS of the different atoms forming the two interface layers. The electric polarization and the different relaxation of the O atoms at the interfaces IF1 and IF2 result in a difference of charge transfer and hybridization between the O-p and Ni-d orbitals, as confirmed by the variation of the atomic spin moments and Mulliken charges reported in Table. S1. Because we choose to model both interfaces with the Ni electrode by a full oxygen layer composed of two O1 and two O2 atoms, the whole HfO_2 film is not stoichiometric by construction, which explains the shift of the Fermi level toward lower energies. The LDOSs show that the Ni bands at IF1 are more depopulated than at IF2, and that their hybridization with the orbitals of O1 is stronger than with O2 at this interface, while it is almost equivalent for the two types of oxygen atoms at IF2. This difference of charge transfer between the two interfaces is responsible for a variation of the local magnetic moment of 1.44 μ_{B} per interface area (see Table S1 [25]), characteristic of the emergence of a magnetoelectric coupling, as discussed in Sec. SII B [25]. The data displayed in Fig. S2 [25] shows that the variation of charge transfer and local spin magnetic moment is not linear as a function of P; as explained below, these properties mostly depend on the position of the O1 atoms located at the interface.

Because of the difference of orbital overlaps between the two interfaces, i.e., when P is reversed, it is also expected that the magnetocrystalline anisotropy energy (MCAE) varies upon switching the electric polarization. We find that, for the whole supercell, the easy axis is oriented along the [001] direction, with a total MCAE of -13.6, -23.7, and -18.9 meV nm^{-2} with respect to the [010], [100], and [110] axes, respectively. In Fig. 2(a), we report the layer projection of the MCAE, $\Delta E_l^{\mathrm{SOC}}$, in order to distinguish the individual contribution of each Ni/HfO_2 interface. Whereas, in the center of the Ni layer, $\Delta E_l^{\mathrm{SOC}}$ remains slightly negative ($\simeq -1.3$ meV nm^{-2} with the [110] direction, close from the

TABLE I. Magnetocrystalline anisotropy energies calculated at various metal/ferroelectric interfaces and their variations upon electric-polarization reversal. The values are given for a metal-layer thickness of approximately four atomic monolayers.

Interface	MCAE (meV nm^{-2})		
	$P\uparrow$	$P\downarrow$	Δ MCAE
Fe/$BaTiO_3$ [28]	−8.3	−6.3	−2.0
Co/Pb(Zr,Ti)O_3 [29]	11.2	6.8	4.4
Co/PVDF [30]	−1.75	−2.6	0.85
Ni/HfO_2 (This work)	−6.0	−11.9	5.9

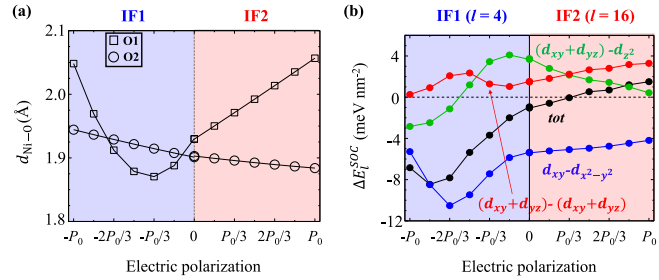

FIG. 3. Variation of the (a) chemical bond lengths d between the nearest Ni and O atoms and (b) MCAE projected on the interface Ni layers, with the corresponding main d-d contributions.

value of −1.5 meV nm^{-2} calculated for strained bulk Ni), it displays strong variations in the two Ni atomic layers at the interface, with a decrease down to $\Delta E_4^{SOC} = -6.8$ meV nm^{-2} at IF1 ($l = 4$), and an increase up to the positive value of $\Delta E_{16}^{SOC} = +1.4$ meV nm^{-2} at IF2 ($l = 16$). At IF1, we thus predict that the perpendicular magnetic anisotropy (PMA) is reinforced, whereas it is weakened at IF2, enabling a net in-plane magnetic anisotropy. As shown in Fig. S4, even if the magnitude of the local MCAE at the interface depends on the strain, we demonstrated that the reversal of its sign with P is preserved even in the absence of tensile strain in the Ni layer. To assess the overall impact of ferroelectricity on the MCAE, we define the anisotropy modulation as $\Delta E_P^{SOC} = \sum_{i=1}^{4} \Delta E_i^{SOC} - \sum_{i=16}^{20} \Delta E_i^{SOC}$. We find that reversing the ferroelectric polarization results in a change of MCAE of about $\Delta E_P^{SOC} = 5.9$ meV nm^{-2} (8 meV nm^{-2}) for the [110] ([100]) direction. This modification is remarkably large as it is comparable to the PMA of Fe/MgO interfaces (≈8.5 meV nm^{-2}) [26] and is of the same order as the voltage-controlled MCAE change reported by Bauer *et al.* [27] or calculated at other metal/ferroelectric interfaces (See Table I). This efficient ferroelectric tuning of the magnetic anisotropy opens inspiring perspectives for low-energy control of magnetism.

This strong variation of the MCAE stems from the dramatic impact of the ferroelectricity on the hybridization between Ni-3d and O-2p orbitals (see Fig. S2 and S3 from the Supplemental Material [25]) and charge transfer through lattice distortions, responsible for the calculated changes of the d-d contributions to the spin-orbit energy. From Fig. 2(b), we can indeed see that the strong contribution toward the PMA ($\Delta E_l^{SOC} < 0$) in the IF1($l = 4$) layer is mostly due to matrix elements corresponding to the contribution involving d_{xy} and $d_{x^2-y^2}$ orbitals. At IF2($l = 16$), the magnitude of the contributions between the d_{xy} and $d_{x^2-y^2}$ orbitals is decreased, when compared with those calculated at IF1, and we observe at the same time an increase of the positive contributions between d_{z^2} and d_{xz}, d_{yz} orbitals, which become dominant. According to the projected DOS displayed in Fig. S3(b), the states for which these orbital contributions are mainly formed strongly hybridize with O-($p_x + p_y$) orbitals.

To describe how the MCAE varies with the Ni-O interatomic distances at the interface, we compute these interface properties as a function of the electric polarization. To do so, as explained in details in Sec. SI B [25], we compute the MCAE for different structures generated by linearly interpolating the atomic positions between a supercell with a centrosymmetric HfO_2 film, in which the atomic positions have been kept fixed inside the hafnia film and relaxed at the interface and in the Ni layer, and the fully optimized polar structure. From the structural optimization, we found that the linear variation of P from $-P_0$ to $+P_0$ modeled with this method also induces a linear variation of the averaged out-of-plane Ni-O1 and Ni-O2 distances at the Ni/HfO_2 interface (not shown). As illustrated in Fig. 3(a), if the variation of the averaged Ni-O chemical bond lengths remains linear with O2 atoms in the whole range of polarization, we observe a nonlinear variation with the polar O1 atoms when the polarization is negative, which is a consequence of an additional relative displacement of the Ni/O atoms along the [100] axis. With this in-plane displacement, the interface Ni atoms that are initially located in a bridge position, i.e., with two oxygen atoms as first neighbors, move in a hollow position and get closer to a third oxygen atom at the interface IF1. The averaged Ni-O bond length then passes by a minimum of $d_{Ni\text{-}O1} = 1.87$ Å for $P = -P_0/3$ and reaches two maxima of $d_{Ni\text{-}O1} = 2.05$ Å at $P = -P_0$ and $d_{Ni\text{-}O1} = 2.06$ Å at $P = +P_0$. The Ni-O distances at the interfaces correlates with the variations of the local MCAE, as shown in Fig. 3(b). Similarly, the MCAE increases linearly between 0 and $+P_0$ and is nonlinear for negative electric polarization at IF1. The variation of MCAE can also be correlated, according to the model presented in Ref. [31] with the variation of $\Delta m_L = m_L^{001} - m_L^{110}$ given in Fig. S2b, which also displays a change of its sign when P is reversed. The change of ΔE_l^{SOC} is mostly dominated by the change of the negative contribution between d_{xy} and $d_{x^2-y^2}$ orbitals and positive contribution between d_{xz} and d_{yz} orbitals. The decrease of these values when P decreases favors the stabilization of the PMA, but is accompanied by an increase of the (d_{xz}, d_{yz})-d_{z^2} matrix elements, which has the opposite effect.

Besides the ferroelectric control of the MCAE, reversing the ferroelectric polarization is also expected to massively impact the spin and orbital textures at the interface, which is of direct interest to spin-charge and orbital-charge interconversion [3,32]. As a matter of fact, the inversion symmetry breaking at the interface promotes an orbital texture that is odd in momentum (see Fig. S6 [25]). In the presence of spin-orbit coupling, this orbital texture is accompanied by a spin texture [33] that unlock the so-called inverse spin [34] and orbital

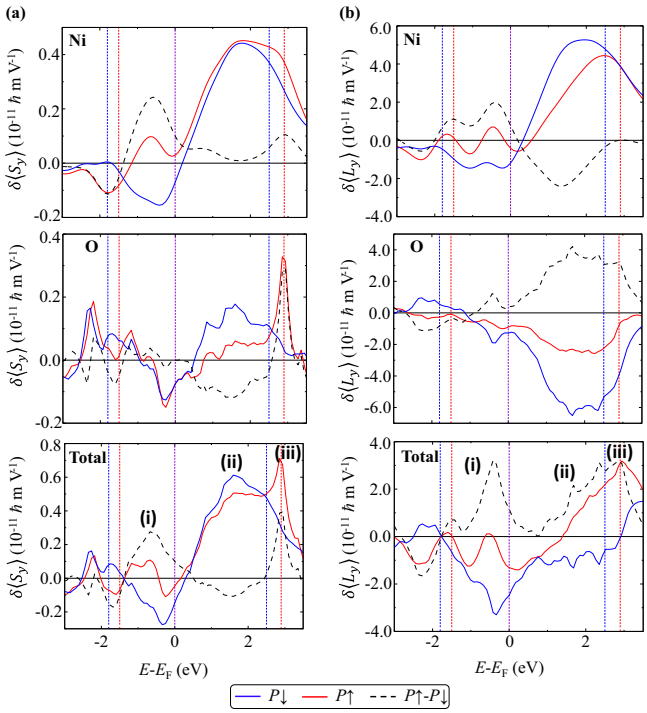

FIG. 4. Spin (a) and orbital (b) responses to an in-plane electric field calculated for a top Ni electrode. The response for an outward(inward) electric polarization $P\uparrow(P\downarrow)$ is calculated considering the contribution of the interface IF2 (IF1, multiplied by -1). More details are given in Sec. SI D and SIII from the Supplemental Material [25]). The dashed black lines correspond to the difference of both responses, i.e., $2\delta\langle S_y\rangle_P$ (a) and $2\delta\langle L_y\rangle_P$. The red and blue dotted lines show the limits of the local HfO_2 band gap in the vicinity of the two interfaces.

[35] Edelstein effects, i.e., the generation of a spin and orbital density induced by a charge current. Switching the ferroelectric polarization is expected to modify the orbital hybridization between O1 and Ni at the interface and thereby tune both inverse spin and orbital Edelstein effects. We compute the nonequilibrium spin and orbital densities, $\delta\langle S_y\rangle$ and $\delta\langle L_y\rangle$, using the Kubo formula within the linear-response theory [36] (more details are given in the Supplemental Material [25]). Since the noncentrosymmetric spin and orbital textures are well localized at the interface, as confirmed by Fig. S5 [25], we focus our attention on the contributions coming from Ni and O1 atoms at IF1 and IF2. Because the calculated densities depend on the energy of the Fermi level, we also restrict our study to an energy window delimited by the band gap of HfO_2 in the vicinity of the two interfaces, i.e., between $-1.8(-1.5)$ eV and $+2.5(+2.9)$ eV at IF1(IF2), where only the bands of Ni and O participate to the transport properties (See Fig. 1(b) and Fig. S1 [25]).

Figure 4 displays both spin and orbital densities, $\delta\langle S_y\rangle$ and $\delta\langle L_y\rangle$, for the electric polarization pointing outward (P ↑, red lines) and inward (P ↓, blue lines). If the slab were perfectly symmetric, and if the electric polarization did not have any influence, $\delta\langle S_y\rangle$ (and $\delta\langle L_y\rangle$) would be equal for P ↑ and P ↓. The influence of the electric polarization can be

TABLE II. Antisymmetric and symmetric parts of the spin and orbital densities at Fermi level. The unit is $10^{-11}\hbar$ m V^{-1}.

	$\delta\langle S_y\rangle_0$	$\delta\langle S_y\rangle_P$	η_S (%)	$\delta\langle L_y\rangle_0$	$\delta\langle L_y\rangle_P$	η_L (%)
Ni	−0.02	0.05	−250	−0.96	0.21	−22
O	−0.074	0	0	−1.09	0.19	−17
Total	−0.092	0.05	−53	−1.9	0.6	−32

analyzed by parsing the density into a symmetric, $\delta\langle S_y\rangle_0 = (\delta\langle S_y\rangle_{P\uparrow} + \delta\langle S_y\rangle_{P\downarrow})/2$, and an antisymmetric part, $\delta\langle S_y\rangle_P = (\delta\langle S_y\rangle_{P\downarrow} - \delta\langle S_y\rangle_{P\uparrow})/2$, the latter being directly associated with the electric polarization. A similar definition applies to the orbital density $\delta\langle L_y\rangle$. In Table II, we report the values of the symmetric and antisymmetric parts of the spin and orbital densities at Fermi level. We find that the average spin density located on the interfacial Ni is $\delta\langle S_y\rangle_0 = -2\times10^{-13}\hbar$ m V^{-1}, which, using a free electron model [34] with a lattice constant of 2.5 Å, corresponds to an effective Rashba strength of $\sim10^{-13}$ eV m. Upon reversing the ferroelectric polarization, the modulation of the spin density amounts to $\delta\langle S_y\rangle_P = 5\times10^{-13}\hbar$ m V^{-1}, which corresponds to a giant modulation $\eta_S = \delta\langle S_y\rangle_0/\delta\langle S_y\rangle_P = -250\%$. Interestingly, the spin density at the Fermi level on the O1 atoms near the interface is unaffected by the polarization. Summing both contributions, the total spin density at the interface can be modulated by about $\eta_S \approx 53\%$. As a comparison, Mishra *et al.* [37] recently demonstrated that in Pt/Co(d)/GdOx thin films, the Rashba field H_R/j_e could be modulated from −500 to +250 Oe A^{-1} m^2 by voltage-driven oxygen migration. The corresponding modulation of the spin density can be obtained using $S = (dM_s/\Delta)H_R/j_e$ [38], where $d = 0.8$ nm and $M_s = 1400$ kA m^{-1} are the thickness and saturation magnetization of the Co layer, and Δ is the exchange energy (≈2 eV). Using these parameters, we find that the spin density is tuned between -10 and $+5\times10^{-13}\hbar$ m V^{-1}, which compares favorably with our prediction.

The orbital densities displayed in Fig. 4(b) are about one order of magnitude larger than the spin density, in agreement with the literature [8,9,39]. At Fermi level, we obtain an average interfacial orbital density of about $-1.9\times10^{-11}\hbar$ m V^{-1}, which is comparable to the orbital densities obtained at transition metal interfaces [40] and one order of magnitude smaller than the giant orbital density found at Al/Co interfaces [41]. The ferroelectric modulation of the orbital densities is about 32%, which is remarkable.

Away from Fermi level, the spin and orbital densities display two extrema, labeled (i) and (ii) around energies of approximately −0.6 eV and +1.7 eV, which also correspond to a maximal modulation upon polarization reversal. For energies below E_F, the bands have a predominant Ni-d character and the calculated spin and orbital responses are moderate. This means that although Ni-d states provide reasonably large spin and orbital projections around the Fermi level, their higher localized nature limits their overall magnitude. This is in contrast with the densities observed around (ii), where sp bands predominate, leading to enhanced responses, in agreement with the large value of the longitudinal conductivity σ_{xx}, as shown in Fig. S7 [25]. We notice a narrowing of the spin density peak (ii), when switching from P ↓ to P ↑, and a

shift in energy of the maximum of the orbital response, from $E_F + 1.93$ eV to $E_F + 2.47$ eV, which follows the shift of the electric potential and the response contribution of Ni atoms. A third maximum (iii) in the spin and orbital responses can also be noticed at $E \sim E_F + 2.9$ eV; such an energy corresponds to the local conduction band minimum of HfO_2 for the P ↑ configuration (IF2 interface), where the oxygen atoms interact more strongly with Hf atoms due to their larger proximity in energy, enhancing the spin-orbit interaction and, consequently, the spin density. This peak is shifted toward higher energies and decreases in magnitude upon polarization switching. At $P = -P_0$, the peak completely disappears because of the too large Hf-O1 distance for the P ↓ configuration (IF1 interface - see Fig. S8 [25]).

In summary, we have found that the spin and orbital properties at Ni/HfO_2 interface can be controlled through the ferroelectric polarization via the modulation of the Ni-O bond length. Remarkably, our calculations suggest that the MCAE can be switched from in-plane to out-of-plane upon reversing the electric polarization. At the same time, the spin and orbital textures at Fermi level are also substantially tuned, resulting in modulations of the spin-charge and orbital-charge interconversion efficiency of several tens of percent. This finding makes Ni/HfO_2 particularly appealing for voltage-controlled memory and logic devices. To fully assess the suitability of this material for MESO [2], FESO [3] or SOT-MRAM [4], a comprehensive evaluation of energy consumption should be conducted taking into account not only the robustness of the magnetoelectric effects discussed here with the oxidation states of the interface [21,42–46], but also the magnitude of the voltage required to switch the ferroelectric polarization, as well as the time scale of the operation [21,42–46].

This work was supported by the ANR ORION project, Grant No. ANR-20-CE30-0022-01 of the French Agence Nationale de la Recherche, by the Excellence Initiative of Aix-Marseille Université-A*Midex, a French "Investissements d'Avenir" program, by the France 2030 government Grants managed by the French National Research Agency PEPR SPIN [SPINMAT] ANR-22-EXSP-0007 and [SPINTHEORY] ANR-22-EXSP-0009 and by the EIC Pathfinder OPEN Grant No.101129641 "OBELIX". This work was granted access to the HPC resources of CALMIP (Allocations No. 2022-2024/P19004 and No. P1229) and CINES (Allocation No. AD010915807R1).

Data availability. The data that support the findings of this article are not publicly available upon publication because it is not technically feasible and/or the cost of preparing, depositing, and hosting the data would be prohibitive within the terms of this research project. The data are available from the authors upon reasonable request.

[1] V. Garcia, M. Bibes, and A. Barthélémy, Artificial multiferroic heterostructures for an electric control of magnetic properties, C. R. Phys. **16**, 168 (2015).

[2] S. Manipatruni, D. E. Nikonov, C.-C. Lin, T. A. Gosavi, H. Liu, B. Prasad, Y.-L. Huang, E. Bonturim, R. Ramesh, and I. A. Young, Scalable energy-efficient magnetoelectric spin-orbit logic, Nature (London) **565**, 35 (2019).

[3] P. Noël, F. Trier, L. M. V. Arche, J. Bréhin, D. C. Vaz, V. Garcia, S. Fusil, A. Barthélémy, L. Vila, M. Bibes, and J.-P. Attané, Non-volatile electric control of spin-charge conversion in a $SrTiO_3$ Rashba system, Nature (London) **580**, 483 (2020).

[4] A. Manchon, J. Železný, I. M. Miron, T. Jungwirth, J. Sinova, A. Thiaville, K. Garello, and P. Gambardella, Current-induced spin-orbit torques in ferromagnetic and antiferromagnetic systems, Rev. Mod. Phys. **91**, 035004 (2019).

[5] H. Mirhosseini, I. V. Maznichenko, S. Abdelouahed, S. Ostanin, A. Ernst, I. Mertig, and J. Henk, Toward a ferroelectric control of Rashba spin-orbit coupling: Bi on $BaTiO_3$(001) from first principles, Phys. Rev. B **81**, 073406 (2010).

[6] M. Fang, Y. Wang, H. Wang, Y. Hou, E. Vetter, Y. Kou, W. Yang, L. Yin, Z. Xiao, Z. Li, L. Jiang, H. N. Lee, S. Zhang, R. Wu, X. Xu, D. Sun, and J. Shen, Tuning the interfacial spin-orbit coupling with ferroelectricity, Nat. Commun. **11**, 2627 (2020).

[7] S. Varotto, L. Nessi, S. Cecchi, J. Sławińska, P. Noël, S. Petrò, F. Fagiani, A. Novati, M. Cantoni, D. Petti, E. Albisetti, M. Costa, R. Calarco, M. B. Nardelli, M. Bibes, S. Picozzi, J.-P. Attané, L. Vila, R. Bertacco, and C. Rinaldi, Room-temperature ferroelectric switching of spin-to-charge conversion in germanium telluride, Nat. Electron. **4**, 740 (2021).

[8] D. Go, D. Jo, T. Gao, K. Ando, S. Blügel, H.-W. Lee, and Y. Mokrousov, Orbital Rashba effect in a surface-oxidized Cu film, Phys. Rev. B **103**, L121113 (2021).

[9] S. Krishnia, B. Bony, E. Rongione, L. M. Vicente-Arche, T. Denneulin, A. Pezo, Y. Lu, R. E. Dunin-Borkowski, S. Collin, A. Fert, J.-M. George, N. Reyren, V. Cros, and H. Jaffrès, Quantifying the large contribution from orbital Rashba-Edelstein effect to the effective damping-like torque on magnetization, APL Mater. **12**, 051105 (2024).

[10] A. Pezo, D. G. Ovalle, and A. Manchon, Orbital Hall effect in crystals: Interatomic versus intra-atomic contributions, Phys. Rev. B **106**, 104414 (2022).

[11] A. Pezo, D. G. Ovalle, and A. Manchon, Orbital Hall physics in two-dimensional Dirac materials, Phys. Rev. B **108**, 075427 (2023).

[12] A. Johansson, B. Göbel, J. Henk, M. Bibes, and I. Mertig, Spin and orbital Edelstein effects in a two-dimensional electron gas: Theory and application to $SrTiO_3$ interfaces, Phys. Rev. Res. **3**, 013275 (2021).

[13] T. P. Ma and J.-P. Han, Why is nonvolatile ferroelectric memory field-effect transistor still elusive?, IEEE Electron Device Lett. **23**, 386 (2002).

[14] T. S. Böscke, J. Müller, D. Bräuhaus, U. Schröder, and U. Böttger, Ferroelectricity in hafnium oxide thin films, Appl. Phys. Lett. **99**, 102903 (2011).

[15] M. H. Park, Y. H. Lee, H. J. Kim, Y. J. Kim, T. Moon, K. D. Kim, J. Müller, A. Kersch, U. Schroeder, T. Mikolajick, and C. S. Hwang, Ferroelectricity and antiferroelectricity of doped thin HfO_2-based films, Adv. Mater. **27**, 1811 (2015).

[16] M. H. Park, T. Schenk, C. M. Fancher, E. D. Grimley, C. Zhou, C. Richter, J. M. LeBeau, J. L. Jones, T. Mikolajick, and U.

Schroeder, A comprehensive study on the structural evolution of HfO_2 thin films doped with various dopants, J. Mater. Chem. C **5**, 4677 (2017).

[17] Y. Yun, P. Buragohain, M. Li, Z. Ahmadi, Y. Zhang, X. Li, H. Wang, J. Li, P. Lu, L. Tao, H. Wang, J. E. Shield, E. Y. Tsymbal, A. Gruverman, and X. Xu, Intrinsic ferroelectricity in Y-doped HfO_2 thin films, Nat. Mater. **21**, 903 (2022).

[18] T. Mikolajick, S. Slesazeck, M. H. Park, and U. Schroeder, Ferroelectric hafnium oxide for ferroelectric random-access memories and ferroelectric field-effect transistors, MRS Bull. **43**, 340 (2018).

[19] W. Banerjee, A. Kashir, and S. Kamba, Hafnium oxide (HfO_2) – A multifunctional oxide: A review on the prospect and challenges of hafnium oxide in resistive switching and ferroelectric memories, Small **18**, 2107575 (2022).

[20] Y. Wei, S. Matzen, C. P. Quinteros, T. Maroutian, G. Agnus, P. Lecoeur, and B. Noheda, Magneto-ionic control of spin polarization in multiferroic tunnel junctions, npj Quantum Mater. **4**, 62 (2019).

[21] B. F. Vermeulen, F. Ciubotaru, M. I. Popovici, J. Swerts, S. Couet, I. P. Radu, A. Stancu, K. Temst, G. Groeseneken, C. Adelmann, and K. M. Martens, Ferroelectric control of magnetism in ultrathin HfO_2/Co/Pt layers, ACS Appl. Mater. Interfaces **11**, 34385 (2019).

[22] Q. Yang, L. Tao, Z. Jiang, Y. Zhou, E. Y. Tsymbal, and V. Alexandrov, Magnetoelectric effect at the Ni/HfO_2 interface induced by ferroelectric polarization, Phys. Rev. Appl. **12**, 024044 (2019).

[23] V. Mikheev, R. Mantovan, S. Zarubin, A. Dmitriyeva, E. Suvorova, P. A. Buffat, and A. V. Zenkevich, Search for magnetoelectric coupling at the $^{57}Fe/Hf_{0.5}Zr_{0.5}O_2$ interface using operando synchrotron Mössbauer spectroscopy, Adv. Mater. Interfaces **9**, 2201341 (2022).

[24] Z. He, D. Zou, Q. Yang, T. Duan, Y. Tan, C. Lei, S. Xie, and Y. Liu, Polarization-induced magnetoelectric effect in $Fe_3Ga/HfO_2/Fe_3Ga$ heterojunction, Appl. Phys. Express **16**, 121001 (2023).

[25] See Supplemental Material at http://link.aps.org/supplemental/10.1103/PhysRevB.111.L140405 for more details about the methodology used for the calculations (Sec. SI), the calculated electronic and magnetic properties (Sec. SII), and spin and orbital accumulations (Sec. SIII), which includes Refs. [9,22,47–69].

[26] H. X. Yang, M. Chshiev, B. Dieny, J. H. Lee, A. Manchon, and K. H. Shin, First-principles investigation of the very large perpendicular magnetic anisotropy at Fe|MgO and Co| MgO interfaces, Phys. Rev. B **84**, 054401 (2011).

[27] U. Bauer, L. Yao, A. J. Tan, P. Agrawal, S. Emori, H. L. Tuller, S. van Dijken, and G. S. D. Beach, Magneto-ionic control of interfacial magnetism, Nat. Mater. **14**, 174 (2015).

[28] P. V. Lukashev, J. D. Burton, S. S. Jaswal, and E. Y. Tsymbal, Ferroelectric control of the magnetocrystalline anisotropy of the Fe/$BaTio_3$(001) interface, J. Phys.: Condens. Matter **24**, 226003 (2012).

[29] R. Arras and S. Cherifi-Hertel, Polarization control of the interface ferromagnetic to antiferromagnetic phase transition in Co/Pb(Zr,Ti)O_3, ACS Appl. Mater. Interfaces **11**, 34399 (2019).

[30] P. V. Lukashev, T. R. Paudel, J. M. López-Encarnación, S. Adenwalla, E. Y. Tsymbal, and J. P. Velev, Ferroelectric control of magnetocrystalline anisotropy at cobalt/poly(vinylidene fluoride) interfaces, ACS Nano **6**, 9745 (2012).

[31] P. Bruno, Tight-binding approach to the orbital magnetic moment and magnetocrystalline anisotropy of transition-metal monolayers, Phys. Rev. B **39**, 865(R) (1989).

[32] A. E. Hamdi, J.-Y. Chauleau, M. Boselli, C. Thibault, C. Gorini, A. Smogunov, C. Barreteau, S. Gariglio, J.-M. Triscone, and M. Viret, Observation of the orbital inverse Rashba-Edelstein effect, Nat. Phys. **19**, 1855 (2023).

[33] G. Bihlmayer, P. Noël, D. V. Vyalikh, E. V. Chulkov, and A. Manchon, Rashba-like physics in condensed matter, Nat. Rev. Phys. **4**, 642 (2022).

[34] V. M. Edelstein, Spin polarization of conduction electrons induced by electric current in two-dimensional asymmetric electron systems, Solid State Commun. **73**, 233 (1990).

[35] D. Go, J.-P. Hanke, P. M. Buhl, F. Freimuth, G. Bihlmayer, H.-W. Lee, Y. Mokrousov, and S. Blügel, Toward surface orbitronics: Giant orbital magnetism from the orbital Rashba effect at the surface of *sp*-metals, Sci. Rep. **7**, 46742 (2017).

[36] V. Bonbien and A. Manchon, Symmetrized decomposition of the Kubo-Bastin formula, Phys. Rev. B **102**, 085113 (2020).

[37] R. Mishra, F. Mahfouzi, D. Kumar, K. Cai, M. Chen, X. Qiu, N. Kioussis, and H. Yang, Electric-field control of spin accumulation direction for spin-orbit torques, Nat. Commun. **10**, 248 (2010).

[38] A. Manchon and S. Zhang, Theory of nonequilibrium intrinsic spin torque in a single nanomagnet, Phys. Rev. B **78**, 212405 (2008).

[39] E. Santos, J.E. Abrão, D. Go, L.K. de Assis, Y. Mokrousov, J. B. S. Mendes, and A. Azevedo, Inverse orbital torque via spin-orbital intertwined states, Phys. Rev. Appl. **19**, 014069 (2023).

[40] L. Salemi, M. Berritta, and P. M. Oppeneer, Quantitative comparison of electrically induced spin and orbital polarizations in heavy-metal/3*d*-metal bilayers, Phys. Rev. Mater. **5**, 074407 (2021).

[41] S. A. Nikolaev, M. Chshiev, F. Ibrahim, S. Krishnia, N. Sebe, J.-M. George, V. Cros, H. Jaffrès, and A. Fert, Large chiral orbital texture and orbital Edelstein effect in Co/Al heterostructure, Nano Lett. **24**, 13465 (2024).

[42] A. Dmitriyeva, V. Mikheev, S. Zarubin, A. Chouprik, G. Vinai, V. Polewczyk, P. Torelli, Y. Matveyev, C. Schlueter, I. Karateev, Q. Yang, Z. Chen, L. Tao, E. Y. Tsymbal, and A. Zenkevich, Magnetoelectric coupling at the Ni/$Hf_{0.5}Zr_{0.5}O_2$ interface, ACS Nano **15**, 14891 (2021).

[43] Z. Chen, Q. Yang, L. Tao, and E. Y. Tsymbal, Reversal of the magnetoelectric effect at a ferromagnetic metal/ferroelectric interface induced by metal oxidation, npj Comput. Mater. **7**, 204 (2021).

[44] T. K. Paul, A. K. Saha, and S. K. Gupta, Oxygen vacancy-induced monoclinic dead layers in ferroelectric $Hf_xZr_{1-x}O_2$ with metal electrodes, arXiv:2412.06416.

[45] A. Acosta, J. M. P. Martirez, N. Lim, J. P. Chang, and E. A. Carter, Relationship between ferroelectric polarization and stoichiometry of HfO_2 surfaces, Phys. Rev. Mater. **5**, 124417 (2021).

[46] A. Acosta, J. M. P. Martirez, N. Lim, J. P. Chang, and E. A. Carter, Effect of thickness and surface composition on the stability of polarization in ferroelectric $Hf_xZr_{1-x}O_2$ thin films, Phys. Rev. Mater. **7**, 124401 (2023).

[47] P. E. Blöchl, Projector augmented-wave method, Phys. Rev. B **50**, 17953 (1994).

[48] G. Kresse and D. Joubert, From ultrasoft pseudopotentials to the projector augmented-wave method, Phys. Rev. B **59**, 1758 (1999).

[49] G. Kresse and J. Furthmüller, Efficiency of *ab initio* total energy calculations for metals and semiconductors using a plane-wave basis set, Comput. Mater. Sci. **6**, 15 (1996).

[50] G. Kresse and J. Furthmüller, Efficient iterative schemes for *ab initio* total-energy calculations using a plane-wave basis set, Phys. Rev. B **54**, 11169 (1996).

[51] J. M. Soler, E. Artacho, J. D. Gale, A. García, J. Junquera, P. Ordejón, and D. Sánchez-Portal, The SIESTA method for *ab initio* order-*N* materials simulation, J. Phys.: Condens. Matter **14**, 2745 (2002).

[52] J. P. Perdew, A. Ruzsinszky, G. I. Csonka, O. A. Vydrov, G. E. Scuseria, L. A. Constantin, X. Zhou, and K. Burke, Restoring the density-gradient expansion for exchange in solids and surfaces, Phys. Rev. Lett. **100**, 136406 (2008). Erratum: **102**, 039902(E) (2009).

[53] D.-H. Choe, S. Kim, T. Moon, S. Jo, H. Bae, S.-G. Nam, Y. S. Lee, and J. Heo, Unexpectedly low barrier of ferroelectric switching in HfO_2 via topological domain walls, Mater. Today **50**, 8 (2021).

[54] L. Ma, J. Wu, T. Zhu, Y. Huang, Q. Lu, and S. Liu, Ultrahigh oxygen ion mobility in ferroelectric hafnia, Phys. Rev. Lett. **131**, 256801 (2023).

[55] T. Zhu, L. Ma, S. Deng, and S. Liu, Progress in computational understanding of ferroelectric mechanisms in HfO_2, npj Comput. Mater. **10**, 188 (2024).

[56] S. Steiner, S. Khmelevskyi, M. Marsmann, and G. Kresse, Calculation of the magnetic anisotropy with projected-augmented-wave methodology and the case study of disordered Fe_{1-x} Co_x alloys, Phys. Rev. B **93**, 224425 (2016).

[57] F. Fernández-Seivane, M. A. Oliveira, S. Sanvito, and J. Ferrer, On-site approximation for spin–orbit coupling in linear combination of atomic orbitals density functional methods, J. Phys.: Condens. Matter **19**, 489001 (2007).

[58] N. Troullier and J. L. Martins, Efficient pseudopotentials for plane-wave calculations, Phys. Rev. B **43**, 1993 (1991).

[59] N. Papior *et al.*, zerothi/sisl: v0.15.2 (Version 0.15.2), Zenodo (2024), 10.5281/zenodo.597181.

[60] D. G. Ovalle, A. Pezo, and A. Manchon, Spin-orbit torque for field-free switching in C_{3v} crystals, Phys. Rev. B **107**, 094422 (2023).

[61] L. Liu, A. Pezo, D. G. Ovalle, C. Zhou, Q. Shen, H. Chen, T. Zhao, W. Lin, L. Jia, Q. Zhang, H. Zhou, Y. Yang, A. Manchon, and J. Chen, Crystal symmetry-dependent in-plane Hall effect, Nano Lett. **24**, 733 (2024).

[62] T. D. Huan, V. Sharma, G. A. Rossetti, Jr., and R. Ramprasad, Pathways towards ferroelectricity in hafnia, Phys. Rev. B **90**, 064111 (2014).

[63] Y. Qi, S. Singh, C. Lau, F.-T. Huang, X. Xu, F. J. Walker, C. H. Ahn, S.-W. Cheong, and K. M. Rabe, Stabilization of competing ferroelectric phases of HfO_2 under epitaxial strain, Phys. Rev. Lett. **125**, 257603 (2020).

[64] J. Wang, H. P. Li, and R. Stevens, Hafnia and hafnia-toughened ceramics, J. Mater. Sci. **27**, 5397 (1992).

[65] X. Sang, E. D. Grimley, T. Schenk, U. Schroeder, and J. M. LeBeau, On the structural origins of ferroelectricity in HfO_2 thin films, Appl. Phys. Lett. **106**, 162905 (2015).

[66] M. Dogan, N. Gong, T.-P. Ma, and S. Ismail-Beigi, Causes of ferroelectricity in HfO_2-based thin films: an *ab initio* perspective, Phys. Chem. Chem. Phys. **21**, 12150 (2019).

[67] J. Müller, T. S. Böscke, U. Schröder, S. Mueller, D. Bräuhaus, U. Böttger, L. Frey, and T. Mikolajick, Ferroelectricity in simple binary ZrO_2 and HfO_2, Nano Lett. **12**, 4318 (2012).

[68] M. Hoffmann, U. Schroeder, T. Schenk, T. Shimizu, H. Funakubo, O. Sakata, D. Pohl, M. Drescher, C. Adelmann, R. Materlik, A. Kersch, and T. Mikolajick, Stabilizing the ferroelectric phase in doped hafnium oxide, J. Appl. Phys. **118**, 072006 (2015).

[69] L. L. Tao, T. R. Paudel, A. A. Kovalev, and E. Y. Tsymbal, Reversible spin texture in ferroelectric HfO_2, Phys. Rev. B **95**, 245141 (2017).